Analyzing powers for $^2\mathrm{H}(\vec{d},d)^2\mathrm{H}$ at deuteron energies of 3.0, 4.75, and 6.0 MeV

B. J. Crowe III,* C. R. Brune, W. H. Geist,† H. J. Karwowski, E. J. Ludwig, and K. D. Veal†
Department of Physics and Astronomy, University of North Carolina at Chapel Hill, Chapel Hill, North Carolina 27599-3255 and Triangle Universities Nuclear Laboratory, Durham, North Carolina 27708

A. C. Fonseca
Centro Fisica Nuclear, Universidade de Lisboa, P-1699 Lisbon, Portugal

G. M. Hale
Los Alamos National Laboratory, Los Alamos, New Mexico 87544

K. A. Fletcher
Department of Physics and Astronomy, State University of New York at Geneseo, Geneseo, New York 14454
(Received 29 July 1999; published 17 February 2000)

Tensor analyzing powers for $^2\mathrm{H}(\vec{d},d)^2\mathrm{H}$ elastic scattering were measured at deuteron energies of 3.0, 4.75, and 6.0 MeV. The measured values are below 0.02 and increase with increasing energy. The data were compared to the results of an *R*-matrix parametrization and microscopic four-body calculations. The calculations indicate that the nucleon-nucleon *p* waves have a strong effect on the observables.

PACS number(s): 21.45.+v, 24.70.+s, 25.40.Lw

I. INTRODUCTION

There has been considerable progress made in the last several years in calculating both bound-state and scattering observables for three- and four-nucleon systems. In the case of the three-body system, much has been accomplished using approaches such as direct solutions to the Faddeev equations [1,2] and the expansion of the three-body wave function in terms of pair-correlated hyperspherical harmonics [3]. The success of these methods has been due in no small part to the availability of improved nucleon-nucleon (*NN*) interactions and increased computational capabilities.

Improvements in the theoretical understanding of the four-nucleon system have led to renewed interest in obtaining high-quality experimental data for this system, especially for ^{4}He. At deuteron energies below about 10 MeV, there exist several sets of analyzing power measurements for $^2\mathrm{H}(\vec{d},d)^2\mathrm{H}$. Grüebler *et al.* [4] obtained angular distributions for a complete set of vector (VAP) and tensor (TAP) analyzing power measurements at deuteron energies of 6, 8, 10, and 11.5 MeV. Additional VAP and TAP distributions were obtained at 10 MeV [5], while VAP distributions were completed at 8, 10, and 12 MeV [6] and 10 MeV [7]. Over this energy range, the analyzing powers are quite small, with magnitudes of $\leqslant 0.03$ at most energies. Additional isospin $T=0$ data exist from the p-^{3}H and n-^{3}He channels, compiled in Ref. [8], while experimental investigations of the p-^{3}He channel [9] provide $T=1$ data.

Recently Hofmann and Hale [10] performed microscopic calculations for bound and scattering states of ^{4}He using the resonating group model (RGM) and compared them to the results of a charge-independent, Coulomb-corrected *R*-matrix analysis. Such analysis is hampered by the fact that the energy levels are broad and overlapping, requiring that many observables over a wide range of energies be included in the global parametrization. The *R*-matrix calculations are in agreement with all observables except for the analyzing power T_{22}, where other calculations similarly fail. Also, including the analyzing power data of Ref. [4] in the *R*-matrix analysis produced disagreements with the 2^+ phase shifts predicted by the RGM [13], particularly for the $^3D_2$ phase shifts in the ^{3}He-*n* and ^{3}H-*p* branches. In general, however, the results of the two analyses compare favorably. Important differences appear in channels that can be strongly influenced by the tensor force, and an examination of these differences indicates that a stronger tensor force than that used in Ref. [10] may explain them.

In addition, analyzing power data in this energy regime can be compared to results of microscopic four-body calculations [11]. These comparisons are especially interesting since *d*-*d* elastic scattering should be sensitive to nucleon-nucleon *P*-wave amplitudes and may be sensitive to off-shell and three-body force effects. Encouraged by the theoretical progress, and the need for additional high-accuracy data over a more extended energy range, we have measured angular distributions of analyzing powers in *d*-*d* elastic scattering at 3.0 and 4.75 MeV. We have also obtained T_{20} and T_{22} at 6 MeV to check the discrepant experimental results reported in Ref. [4] at that energy. The present data provide a simpler test of theoretical predictions of *d*-*d* scattering observables than data at higher energy since fewer partial waves are important.

II. EXPERIMENTAL TECHNIQUES

All measurements were performed at the Triangle Universities Nuclear Laboratory. The polarized deuteron beams

*Present address: Shaw University, Raleigh, NC 27601.

†Present address: Los Alamos National Laboratory, Los Alamos NM 87544.

were provided by the high-intensity Atomic Beam Polarized Ion Source [12] and accelerated through a 10 MV FN Tandem accelerator to a 62-cm-diameter scattering chamber. Typical beam currents of 100 nA were incident on target. The analyzing powers T_{20} and T_{22} were measured at $E_d = 3.0$, 4.75, and 6.0 MeV, while the analyzing powers iT_{11} and T_{21} were measured at $E_d = 4.75$ MeV. All data were taken over an angular range of $40° \leqslant \theta_{\text{c.m.}} \leqslant 110°$. For the analyzing power measurements, RF transition units were used at the source to populate two hyperfine states of atomic deuterium which can produce maximum theoretical tensor polarizations $p_{zz} = \pm 1$ and pure maximum vector polarizations of $p_z = \pm 2/3$. The beam polarization was monitored online using the $^3\text{He}(\vec{d},p)^4\text{He}$ reaction in a polarimeter [14] positioned directly behind the scattering chamber. Typical measured tensor and vector polarizations were $P_{zz} \approx \pm 0.7$ and $P_z \approx \pm 0.5$. The systematic uncertainty in the tensor and vector polarizations is estimated to be 4%.

The polarization data were taken using three spin states: an unpolarized state (state 1), a positive polarized state (state 2), and a negative polarized state (state 3). A Wien filter was used to set the spin axis relative to the reaction plane. A fast spin-flip scheme was employed so that the desired hyperfine states of deuterium were cycled approximately once every second. This technique allowed data from each spin state to be collected almost simultaneously so that slow changes in the beam position, amplifier gain, and target thickness would affect all spectra in the same way.

Thin deuterated-carbon targets [15] were used which consisted of $\approx 2 \times 10^{18}$ and 1×10^{18} atoms/cm^2 of carbon and deuterium, respectively. The deuteron beams lose ≈ 8 keV at an energy of 3.0 MeV in the target. Reaction products were viewed by two pairs of symmetrically placed left and right ΔE-E telescopes containing silicon surface-barrier detectors. The ΔE detectors had thicknesses of 6 and 16 μm for 3.0 and 4.75 MeV data and 19 and 27 μm for 6.0 MeV data. The 300-μm E detectors completely stopped the scattered deuterons at 3.0 and 4.75 MeV, while 500-μm E detectors were used to stop the particles at 6.0 MeV. The telescopes were separated by 20° and subtended solid angles of 4 msr. Sample ΔE-E and total energy spectra are shown in Figs. 1 and 2, respectively. Tests for false asymmetries were carried out by measuring $^{197}\text{Au}(\vec{d},d)$ scattering at $\theta_{\text{lab}} = 40°$ under identical conditions as the d-d measurements. It has been shown [16] that the expected analyzing power for ^{197}Au in this energy range is $< 10^{-4}$. The results were consistent with zero at the level of 5×10^{-4}, the statistical uncertainty of the experiment.

The counts in the left and right detector telescopes were combined in order to determine the analyzing powers. This technique was employed to eliminate contributions from beam moments it_{11} and t_{21} and from the first order effects from left-right shifts on target. The A_{zz} results were obtained from measurements with the spin axis set parallel to the incident beam axis ($\beta = 0°$) and using the expression

$$A_{zz} = \frac{2(r-1)}{p_{zz}^{(2)} - r p_{zz}^{(3)}}, \tag{1}$$

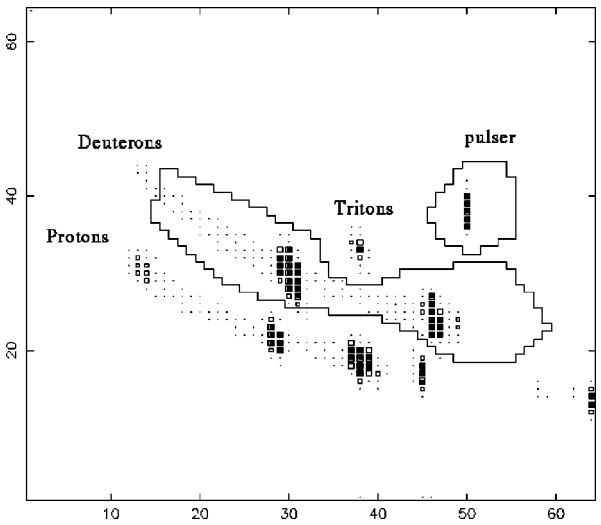

FIG. 1. A plot of energy loss in the ΔE detector versus that in the E detector for particles observed in $^2\text{H}(\vec{d},d)^2\text{H}$ elastic scattering at 4.75 MeV. The outlined area shows the gate used to sort the deuterons of interest into the energy spectrum.

where

$$r = \frac{L^{(2)} + R^{(2)}}{L^{(3)} + R^{(3)}} N, \tag{2}$$

and $p_{zz}^{(i)}$ are beam polarizations. The normalization factor N takes into account the dead-time corrections and the total charge accumulated for both polarization states, and $L^{(i)}$ and $R^{(i)}$ are the ratios of polarized to unpolarized counts in the left and right detectors, respectively. The superscripts represent the polarization states. The expression for A_{yy} is the same, except the A_{yy} data are taken with the spin axis set perpendicular to the beam axis ($\beta = 90°$) and reaction plane.

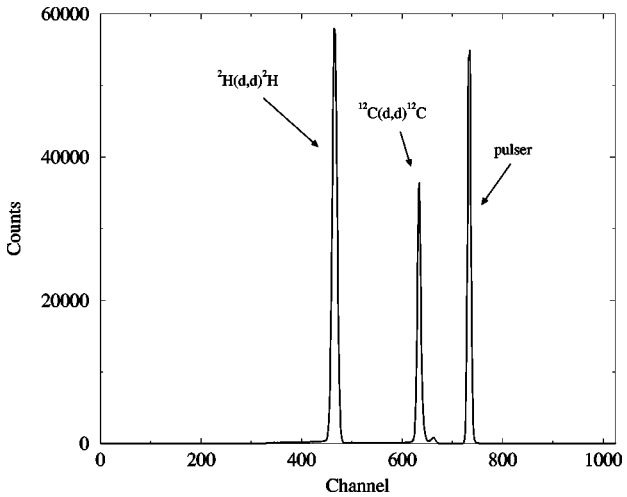

FIG. 2. A spectrum of deuterons observed in $^2\text{H}(\vec{d},d)^2\text{H}$ taken at $E_d = 4.75$ MeV and $\theta_{\text{lab}} = 35°$. The peak at the right is the pulser. The reduced amplitude of the $^{12}\text{C}(\vec{d},d)^{12}\text{C}$ peak is due to hardware prescaling.

The A_{xz} and A_y data, on the other hand, were obtained from measurements using the expressions

$$A_{xz}=\frac{L-R}{p_{zz}}, \tag{3}$$

$$A_y=\frac{L-R}{3p_z}, \tag{4}$$

where L and R are the ratios of polarized to unpolarized counts in the left and right detectors. The results for spin states 2 and 3 were averaged to yield the final result. To measure A_{xz}, the spin axis was set to $\beta=45°$ and in the reaction plane while the A_y data were measured with the same spin axis setting as the A_{yy} data ($\beta=90°$).

From these data, the spherical analyzing powers iT_{11}, T_{20}, T_{21}, and T_{22} were obtained using the following expressions:

$$iT_{11}=\sqrt{\frac{3}{2}}A_y, \tag{5}$$

$$T_{20}=\frac{1}{\sqrt{2}}A_{zz}, \tag{6}$$

$$T_{21}=\frac{-1}{\sqrt{3}}A_{xz}, \tag{7}$$

$$T_{22}=\frac{-1}{\sqrt{3}}\left(A_{yy}+\frac{1}{2}A_{zz}\right). \tag{8}$$

III. THEORY

The theoretical predictions compared to the analyzing power data for $^2\mathrm{H}(\vec{d},d)^2\mathrm{H}$ elastic scattering were obtained from two sources: an R-matrix parametrization and microscopic four-body calculations.

A. *R* matrix

The R matrix predictions are from a global parametrization of the $A=4$ system which has been Coulomb corrected and is charge independent. The analysis includes data from total and differential cross sections, tensor and vector analyzing powers, and polarization-transfer coefficients for processes listed in Ref. [10] along with the present $E_d=3.0$ and 4.75 MeV data. The R-matrix elements are given by

$$R_{c',c}=\sum\frac{\gamma^T_{\lambda c'}\gamma^T_{\lambda c}}{E_\lambda-E}, \tag{9}$$

where $\gamma^T_{\lambda c'}$ are the reduced-width amplitudes and E_λ are the energies for the reaction channel c and energy level λ. These parameters are adjusted to obtain simultaneously the best fit to all the available data for the $A=4$ system below 20 MeV excitation energy.

The reduced-width amplitudes have definite isospins that are restricted to 0 or 1. The $T=1$ parameters are obtained from an analysis of the p-^{3}He scattering data, which reproduces the proton data below 20 MeV. These parameters were used to calculate cross sections and S-wave scattering lengths for n-^{3}H data by Coulomb-energy shifting the eigenenergies E_λ. The $T=0$ parameters are varied to fit the data and are subject to the constraint $\gamma_{p\text{-}^3\mathrm{He}}=-\gamma_{n\text{-}^3\mathrm{H}}$ in isospin-zero levels, which is required by isospin conservation.

B. Four-body calculations

The four-body calculations [17] use the integral equations of Alt, Grassberger, and Sandhas (AGS) [18] for the transition operators involving all (2) + (2) and (3) + (1) channels where the numbers in parentheses represent the number of particles involved. For local NN potentials such equations are three-vector variable integral equations which after partial wave decomposition reduce to a set of coupled equations in three continuous scaler variables. Since scattering calculations require a great number of channels, some technical compromises must be made.

The integral equations we solve are obtained from the modified AGS equations [19,20] after one has (a) represented the original NN t matrix by an operator of rank 1; and (b) represented the resulting $3N$ t matrix by a finite rank operator and taken as many terms as needed to reach convergence. The sole approximation in this approach involves a rank 1 representation of the NN t matrix which may be obtained from the well-known method of Ernest, Shakin, and Thaler (EST) [21]. The multiterm representation of the $3N$ t matrix is done using the energy-dependent pole expansion (EDPE) method developed by Sofianos *et al.* [22]. This approximation for the $3N$ t matrix is under control since one may compare the finite rank approximation with the original results for the $3N$ observables (cross sections and analyzing powers), as well as check the convergence rate of $4N$ observables for increasing rank of the $3N$ t matrix representation. Since in the modified AGS equations the (2) + (2) subsystem is treated by convolution, it is calculated exactly. This method was first used by Fonseca [23] in the binding energy calculation of ^{4}He and later confirmed to be accurate by the exact work of Kamada and Glöckle [24]. More recently, benchmark calculations were performed for the $T=1$ system (n-^{3}H scattering) using Malfliet-Tjon and Argonne V14 potentials in NN partial waves corresponding to $^1S_0$ and $^3S_1$-$^3D_1$. Cross sections and phase shifts were compared to the exact work of Ciesielski [25] in the energy range below the breakup threshold. The results of such comparison [26] show excellent agreement between the two calculations (less than 4% discrepancy), where most of the difference may be attributed to the use by Fonseca of a rank one approximation for the NN t matrix. Therefore the $4N$ calculations presented here are the most complete $dd\rightarrow dd$ calculations we know of using the NN interaction with the Bonn-B and Paris potentials in partial waves corresponding to channels $^1S_0$, $^3S_1$-$^3D_1$, $^1P_1$, $^3P_0$, $^3P_1$, and $^3P_2$. The results of the calculations presented below are separated depending on the number of partial waves included. The first two channels

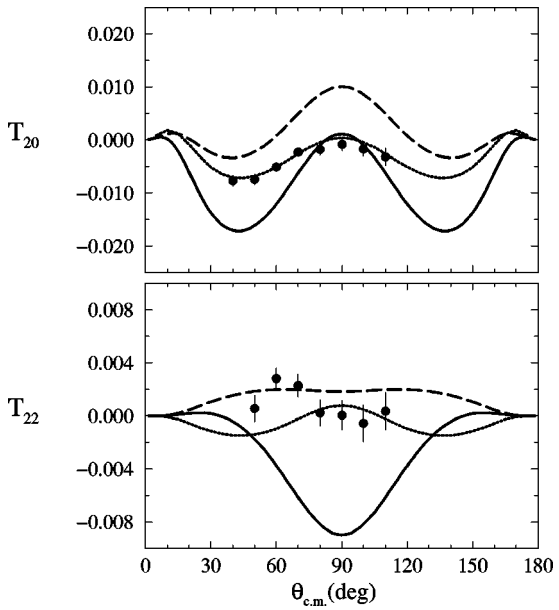

FIG. 3. Tensor analyzing power data obtained for $^2\mathrm{H}(\vec{d},d)^2\mathrm{H}$ at 3 MeV compared to *R*-matrix predictions (dotted curve), and four-body calculations with set A (dashed curve) and set C (solid curve). The error bars in the figure only include counting statistics. At some angles, the error bars are smaller than the experimental points (filled circles).

correspond to including all *NN* partial waves with $j \leqslant 1^+$ and are identified as set A, while the first five channels include all waves with $j \leqslant 1$ (set B), and set C includes the channels of set B plus $^3P_2$. In all calculations we have included all positive and negative parity 3*N* subamplitudes with total angular momentum up to $J^\pi = 7/2^+$ as well as all underlying 3*N* channels corresponding to particle-pair relative orbital angular momentum $L \leqslant 3$. Likewise all (2) + (2) subamplitudes that are consistent with the underlying *NN* channels are included. Finally, all 4*N* observables are calculated using 4*N* amplitudes with total angular momentum up to $\mathcal{J}^\pi = 6^\pm$ in all corresponding (1) + (3) and (2) + (2) channels with relative orbital angular momentum $\mathcal{L} \leqslant 5$.

IV. RESULTS AND DISCUSSION

The TAP's obtained at 3.0, 4.75, and 6.0 MeV are shown in Figs. 3, 4, and 5, respectively, along with *R*-matrix and microscopic four-body calculations with sets A and C discussed above. For identical particles in the exit channel, the TAP's T_{22} and T_{20} must be symmetric around 45° in the lab, which corresponds to a center of mass angle of 90°. The analyzing powers T_{21} and iT_{11} are antisymmetric around the same angle. This allows for an internal consistency check on the experimental data.

The analyzing powers are small but increase as the energy is raised. Variations are small as the energy is changed, which is consistent with expectations of the presence of broad overlapping resonances. In Fig. 5, a comparison is made between the present data and those of Ref. [4]. The present T_{20} angular distribution agrees well with the previous

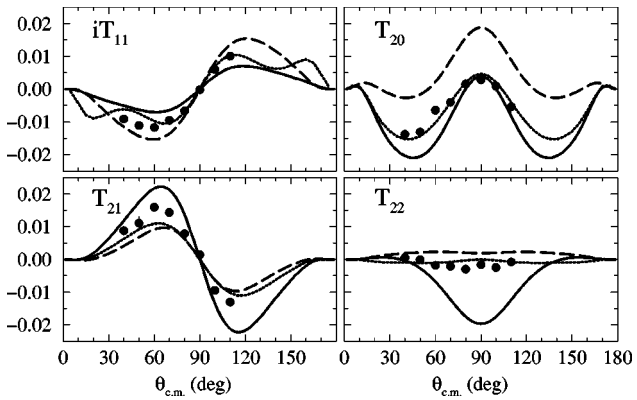

FIG. 4. Vector and tensor analyzing power data for $^2\mathrm{H}(\vec{d},d)^2\mathrm{H}$ at 4.75 MeV compared to *R*-matrix predictions (dotted curve), and four-body calculations with set A (dashed curve) and set C (solid curve). The error bars only include counting statistics. At some angles, the errors bars are smaller than the experimental points (filled circles).

6-MeV result. However, there are disagreements between the two data sets for T_{22} at back angles.

The *R*-matrix parametrization provides a good description of the present data. Both the shapes and the magnitudes of the angular distribution are generally well reproduced.

The results of the 4*N* calculations show general agreement with the data, except for T_{22} at all energies where the full calculation (set C) overshoots the data at 90°. It should be noted that these calculations simultaneously provide a reasonable description of $^2\mathrm{H}(\vec{d},n)^3\mathrm{He}$ and $^2\mathrm{H}(\vec{d},p)^3\mathrm{H}$ tensor observables [17] which are an order of magnitude larger than the tensor observables for the $^2\mathrm{H}(\vec{d},d)^2\mathrm{H}$ reaction. This is by no means a trivial outcome of the calculation given the absence of any adjustable parameters. Therefore we consider

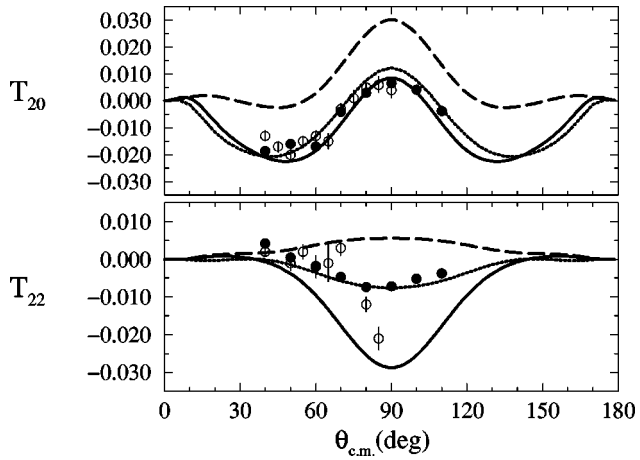

FIG. 5. Tensor analyzing power data for $^2\mathrm{H}(\vec{d},d)^2\mathrm{H}$ at 6.0 MeV obtained in the present study (filled circles) along with comparable data from Ref. [4] (open circles). These data are compared to *R*-matrix predictions (dotted curve), and four-body calculations with set A (dashed curve) and set C (solid curve). The error bars only include counting statistics. At some angles, the errors bars are smaller than the experimental points (filled circles).

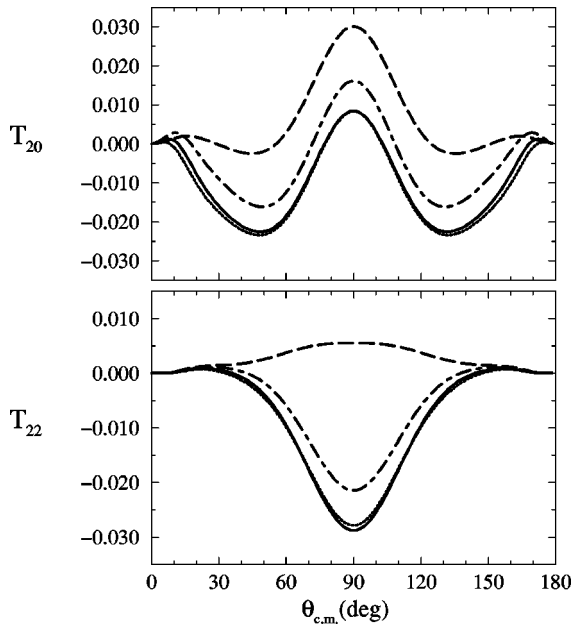

FIG. 6. Four-body calculations of analyzing powers for $^2\mathrm{H}(\vec{d},d)^2\mathrm{H}$ at 6.0 MeV. The dashed curve resulted from calculations including 2*N* partial waves with $j \leqslant 1^+$ (set A in the text), the dotted curve includes partial waves with $j \leqslant 1$ (set B), while the solid curve resulted from set C. The dashed-dotted curve was generated using the Paris potential with set C partial waves.

that the present calculation for $^2\mathrm{H}(\vec{d},d)^2\mathrm{H}$ gives a reasonable description of iT_{11}, T_{20}, and T_{21} data, and provides the correct trend for T_{22} but with too large a magnitude at 90°. We also find that the $^2\mathrm{H}(\vec{d},d)^2\mathrm{H}$ observables are extremely sensitive to the *P*-wave components of the *NN* potentials as shown in Fig. 5. Their presence is responsible for drastic changes in the calculated observables and for improving the overall agreement with the data.

We also find that changing the *NN* input introduces only a small modification in the calculated observables. In Fig. 6, we compare the results of using the Paris potential instead of Bonn-B. Although the effect of changing the *NN* input is larger in 4*N* systems such as $^2\mathrm{H}(\vec{d},d)^2\mathrm{H}$ and $^2\mathrm{H}(\vec{d},p)^3\mathrm{H}$ than in $^1\mathrm{H}(\vec{d},d)^1\mathrm{H}$, one does not find any evidence that a specific interaction is preferred. On the contrary, calculations with both potentials behave essentially in the same manner, in spite of having very different *D*-state probabilities for the deuteron. Therefore any conjectures about extracting the strength of the *NN* tensor force from the data seem premature at this stage.

The 4*N* results shown here for *d*-*d* elastic scattering raise expectations about the possible outcomes of including 3*N* forces and higher partial waves. As discussed in a recent review article on the three-nucleon continuum [2], $^1\mathrm{H}(\vec{d},d)^1\mathrm{H}$ elastic observables (cross sections, vector and tensor polarizations) are insensitive to the choice of a realistic *NN* potential. Beyond the persistent A_y discrepancy at low energies [28], the agreement between calculations and data is excellent in the energy range up to 65 MeV. It is known that the A_y discrepancy at low energies persists even when known static 3*N* force models are added to any realistic *NN* interaction. No matter what choice one takes, the outcome is similar: beyond its effect on the 3*N* binding energy (about 1 MeV more binding), triton wave function related parameters (charge radii, asymptotic normalization constants), and doublet scattering length, all of which correlate almost linearly with the triton binding energy, the 3*N* force plays almost no role in $d+p$ elastic scattering or breakup for deuteron laboratory energies up to $E_d = 65$ MeV. The disagreement we find here in *d*-*d* elastic scattering may not be attributed to the approximations that are used to solve the AGS equations. As mentioned above, the benchmark results [27] for *n*-*t* elastic scattering, using the Argonne V14 potential, indicate that the method is reliable. Therefore, either the discrepancies we find here are resolved by including additional partial waves and a 3*N* force, or new $2N + 3N$ force models have to be invented. In the case of adding a 3*N* force, one uncovers a 3*N* force effect in low-energy scattering that is not associated with scaling with the triton binding energy; in the case of a new nuclear force model, one is confronted with the need for new physics. Either scenario would show the importance of 4*N* scattering as a theoretical laboratory for $2N + 3N$ force model studies.

V. CONCLUSIONS

Angular distributions of analyzing powers for $^2\mathrm{H}(\vec{d},d)^2\mathrm{H}$ have been obtained at 3.0, 4.75, and 6.0 MeV and compared to *R*-matrix and four-body calculations. These angular distributions were obtained at energies lower than any of the previous work. The measured analyzing powers are quite small (<0.02) in this energy range and increase smoothly with increasing energy.

The theoretical calculations generally agree with the data. The *R*-matrix parametrization, which includes the present data set along with data from other reaction and scattering processes, reproduces both the magnitude and shape of the angular distributions. The four-body calculations without *p* waves fail to reproduce the data but with the inclusion of *p* waves the calculations follow the trends of the data in all cases except for the magnitude of the T_{22} data. A lesser disagreement is observed for the T_{21} data.

Future theoretical research should include 3*N* forces as well as higher *NN* partial waves such as $^1D_2$, $^3D_2$, and $^3F_2$ coupled to $^3P_2$ as well as a 3*N* force. Given that the deuterons in the initial and final channels are two large objects, peripheral scattering of nucleons is expected to be enhanced, as the importance of *P*-wave scattering already indicates. Although we anticipate the effect to be small, it should not be neglected given the magnitude of $^2\mathrm{H}(\vec{d},d)^2\mathrm{H}$ observables. The addition of a 3*N* force is also of fundamental importance in order to further test the reliability of present $2N + 3N$ force models. Finally, one may also conjecture that proper inclusion of Coulomb dynamics should also play a role at these energies. Nevertheless, from the experience with $^1\mathrm{H}(\vec{d},d)^1\mathrm{H}$, one expects these effects to be dominant at for-

ward angles and not so much in the angular range of the present data.

One may conclude that present 4*N* calculations with realistic interactions do not reproduce the data as well as the current 3*N* calculations. Unlike $d+n$ scattering where low-energy elastic observables are insensitive to the choice of 2*N* force model or presence of a 3*N* force, 4*N* scattering observables seem to indicate a greater dependency on other factors such as the off-shell *NN* interaction and 3*N* forces.

ACKNOWLEDGMENTS

The authors would like to thank Dr. Zeid Ayer, Dr. Lijuan Ma, Dr. Denise Powell, Dr. Steve Hale, Mike Wood, and Brian Fisher for their help in the data collection process. This work was supported in part by the U.S. Department of Energy under Grant No. DE-FG02-97ER41041. The work of A. C. Fonseca was supported in part by FCT Grant No. PCERN/C/FIS/1157/97.

[1] C. R. Chen, G. L. Payne, J. L. Friar, and B. F. Gibson, Phys. Rev. C **44**, 50 (1991).
[2] W. Glöckle, H. Witala, D. Hüber, H. Kamada, and J. Golak, Phys. Rep. **274**, 107 (1996).
[3] A. Kievsky, M. Viviani, and S. Rosati, Phys. Rev. C **52**, R15 (1995).
[4] W. Grüebler, V. Konig, R. Risler, P. A. Schmelzbach, R. E. White, and P. Marmier, Nucl. Phys. **A193**, 149 (1972).
[5] H. O. Meyer and P. Schiemenz, Nucl. Phys. **A197**, 259 (1972).
[6] G. R. Plattner and L. G. Keller, Phys. Lett. **30B**, 327 (1969).
[7] E. M. Bernstein, G. G. Ohlsen, V. S. Starkovich, and W. G. Simon, Nucl. Phys. **A126**, 641 (1969).
[8] D. R. Tilley, H. R. Weller, and G. M. Hale, Nucl. Phys. **A541**, 1 (1992).
[9] M. T. Alley and L. D. Knutson, Phys. Rev. C **48**, 1901 (1993).
[10] H. M. Hofmann and G. M. Hale, Nucl. Phys. **A613**, 69 (1997).
[11] A. C. Fonseca, Nucl. Phys. **A631**, 675c (1998).
[12] T. B. Clegg, H. J. Karwowski, S. K. Lemieux, R. W. Sayer, E. R. Crosson, W. M. Hooke, C. R. Howell, H. W. Lewis, A. W. Lovette, H. J. Pfutzner, K. A. Sweeton, and W. S. Wilburn, Nucl. Instrum. Methods Phys. Res. A **357**, 200 (1995).
[13] H. Hofmann (private communication).
[14] S. A. Tonsfeldt, T. B. Clegg, E. J. Ludwig, and J. F. Wilkerson, in *Polarization Phenomena in Nuclear Physics*, edited by G. G. Olsen, R. E. Brown, N. Jarmie, W. W. McNaughton, and G. M. Hale, AIP Conf. Proc. 69 (AIP, New York, 1980), p. 961.
[15] T. C. Black, Ph.D. thesis, University of North Carolina at Chapel Hill, 1995 (available from University Microfilms, Ann Arbor, MI 48106).
[16] J. E. Kammeraad and L. D. Knutson, Nucl. Phys. **A435**, 502 (1985).
[17] A. C. Fonseca, Few-Body Syst., Suppl. **10**, 359 (1999).
[18] E. O. Alt, P. Grassberger, and W. Sandhas, Phys. Rev. C **1**, 85 (1970).
[19] A. C. Fonseca and P. E. Shanley, Phys. Rev. D **13**, 2255 (1976); Phys. Rev. C **14**, 1343 (1976).
[20] H. Haberzettl and W. Sandhas, Phys. Rev. C **24**, 359 (1981).
[21] J. Ernest, C. M. Shakin, and R. M. Thaler, Phys. Rev. C **8**, 46 (1973).
[22] S. Sofianos, N. J. McGurk, and H. Fiedeldey, Nucl. Phys. **A318**, 295 (1979).
[23] A. C. Fonseca, Phys. Rev. C **40**, 1390 (1989).
[24] H. Kamada and W. Glöckle, Nucl. Phys. **A548**, 205 (1992).
[25] F. Ciesielski, Ph.D. thesis, Univ. Joseph Fourier, Grenoble, 1997.
[26] J. Carbonell, F. Ciesielski, C. Gignoux, and A. C. Fonseca, Few-Body Syst., Suppl. **10**, 359 (1999).
[27] F. Ciesielski, J. Carbonell, and C. Gignoux, Phys. Lett. B **447**, 199 (1999).
[28] C. R. Brune, W. H. Geist, H. J. Karwowski, E. J. Ludwig, K. D. Veal, M. H. Wood, A. Kievsky, S. Rosati, and M. Viviani, Phys. Lett. B **428**, 13 (1998).